Available online at www.sciencedirect.com
SCIENCE DIRECT
Journal of Sound and Vibration 296 (2006) 968–978
JOURNAL OF SOUND AND VIBRATION
www.elsevier.com/locate/jsvi

Ultrasonic guided wave energy behavior in laminated anisotropic plates

Krishnan Balasubramaniam*, C.V. Krishnamurthy

Centre for Nondestructive Evaluation, Department of Mechanical Engineering, Indian Institute of Technology Madras, Chennai 600 036, India

Received 28 April 2005; received in revised form 1 March 2006; accepted 17 March 2006
Available online 2 June 2006

Abstract

A Gaussian beam model coupled with the transfer-matrix technique, was employed to obtain the internal distributions of the energy vector (also called as power density vector or Poynting vectors) of guided ultrasonic plate waves that are modified due to the anisotropy of the media. The spatial pattern of the energy partitioning of the ultrasonic guided waves, previously called plate-wave-flow-patterns, was predicted from the material properties. The model-based predictions of the plate wave flow patterns in fiber reinforced graphite-epoxy laminates, in the form of gray scale images, compared well with the experimental results. In particular, the observed feature that guided waves in plates with structure-induced anisotropy, such as fiber-reinforced composites, tend to follow preferred directions, is predicted by the model. The model provides further insight into the understanding of the generation and propagation of guided wave mode patterns in structure-induced anisotropic plates. Such studies have potential for application in the area of acoustic emission monitoring, structural health monitoring, and stealth materials development.

1. Introduction

It is well known that in an anisotropic elastic solid, the elastic wave energy propagation vector (also sometimes referred as power density vector, or Poynting vector, or power flow vector) is not necessarily along the elastic wave propagation vector. This effect leads to beam skewing and has been extensively documented in semi-infinite anisotropic media [1–4]. The skewing angle, which is the angle between the energy vector and the wave vector, equals zero when the wave propagates along directions of material symmetry.

In the case of a laminate with multiple layers of materials with the vector of material symmetry not aligned along the same direction (such as for plates made from composite materials using ply lay-up technique), the effect of the energy skew has been reported using plate-wave-flow-patterns [5–8]. It was observed that the fiber directions in multi-layered graphite-epoxy composite plates could be imaged by observing the leaked energy of the guided waves traveling along the plate. The images revealed that the energy of the guided wave propagated across the plate in several spatially distinct directions associated with fiber alignments in various layers. These

*Corresponding author. Tel.: +91 44 2257 8588; fax: +91 44 2257 0545.
E-mail address: balas@iitm.ac.in (K. Balasubramaniam).

0022-460X/$ - see front matter © 2006 Elsevier Ltd. All rights reserved.
doi:10.1016/j.jsv.2006.03.037

directions of energy flow could be correlated with the number of super-layers (a super-layer being a combination of ply groups that can repeat or have mirror images) in the plate. In some cases, weaker energy partitions were also observed in directions not necessarily aligned with the fibers.

In this paper, model based plate-wave-flow-patterns (henceforth referred as PWFP) and comparisons with experimental results are presented. The calculations are carried out by invoking the partial wave superposition principle, for the partial wave power flow vector in individual layers, along with a Gaussian beam model that accounted for the spatial dispersion of energy. The power flow in individual layers from the specified elastic constants and the mutual transfer of energy across layers was modeled using the Thomson–Haskell Transfer-Matrix technique [9–19].

2. Background

Modeling of the reflection/transmission of waves from isotropic multi-layered media has been studied for over four decades, with the work by Thomson [14] setting the stage for the frequently used Thomsen-Haskell Transfer-Matrix technique [15] to transfer boundary conditions from one side of an elastic layer to the other side. A detailed description of the formulation of waves in isotropic layered media can be found in Brekhovskikh [16] and Auld [17]. Rokhlin et al. [18], Nayfeh [19], Ting [20], Mal and Bar-Cohen [21], Hosten [22] and Datta et al. [23] have discussed the extension of the transfer-matrix technique to multi-layered anisotropic media, especially for laminated composites, and correlated theoretical results with experiments. In this paper, the reflected and transmission coefficients for the energy vector (Poynting vector) are obtained by using the transfer-matrix model for a general anisotropic (21 independent elastic constants) multi-layered elastic material system based on the plane wave transfer-matrix method [8].

The traditional technique has certain limitations due to the occurrence of numerical instabilities when analyzing thick, multi-layered structures and intricate anisotropic orientations. A delta-operator technique has been suggested as a remedy [24]. Another recent approach, which reduces the numerical instability, is the stiffness matrix by Wang and Rokhlin [25]. In this paper, a numerical truncation algorithm was successfully employed to avoid the numerical instabilities for the cases investigated [26,27]. The performance of the modified transfer-matrix method, as it was termed, has been compared with the stiffness matrix and the other transfer-matrix techniques [28].

Consider a general anisotropic multi-layered plate immersed in water. The plate consists of an arbitrary number of general anisotropic layers n, rigidly bonded at their interfaces as shown in Fig. 1. Without losing

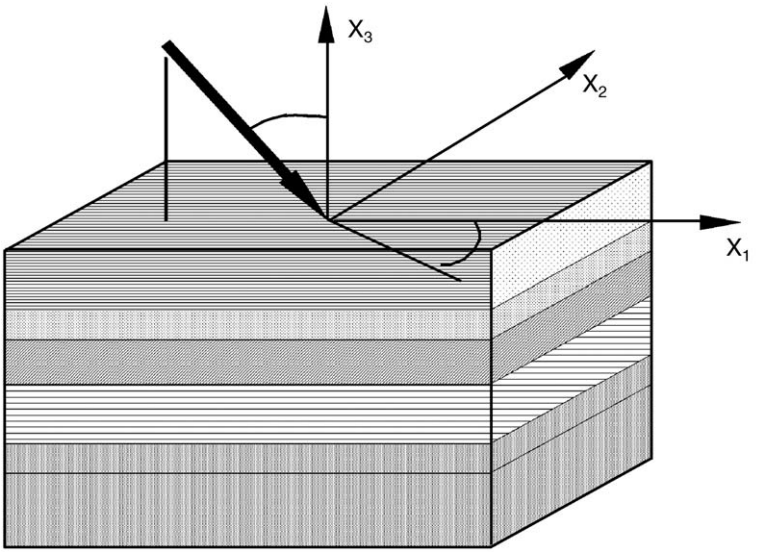

Fig. 1. Representation of the multilayered specimen modeled using the transfer-matrix approach.

generality, it is assumed that leaky plate waves propagate along the x_i direction. The displacements (u_i) of the wave are considered to be in the form:

$$u_i = U_i e^{j(k_i x_i - \omega t)}, \tag{1}$$

where U_i is the amplitude of the displacement, k_i is the wave-vector component, ω is the circular frequency and $i = 1, 2, 3$ refer to the Cartesian components. Based on the Thomson–Haskell transfer-matrix method [14,15], Eq. (2) gives the relationship between the displacements and stresses at the top interface and the bottom interface of the plate.

$$X^t = TX^b, \tag{2}$$

where

$$X^t = \begin{bmatrix} u_1^t & u_2^t & u_3^t & \sigma_{33}^t & \sigma_{23}^t & \sigma_{13}^t \end{bmatrix}^{\mathrm{T}}, \quad X^b = \begin{bmatrix} u_1^b & u_2^b & u_3^b & \sigma_{33}^b & \sigma_{23}^b & \sigma_{13}^b \end{bmatrix}^{\mathrm{T}}.$$

In order to calculate the reflection and transmission coefficients for a plane wave incident on a multi-layered anisotropic plate, a single anisotropic plate between two fluid half spaces must first be considered. In this situation, shear stresses at upper and lower interfaces are zero. Thus, the boundary conditions at the top and the bottom interfaces are given by

$$u_3^{ft} = u_3^t, \quad \sigma_{33}^{ft} = \sigma_{33}^t, \quad \sigma_{13}^t = \sigma_{23}^t = 0, \quad u_3^{fb} = u_3^b, \quad \sigma_{33}^{fb} = \sigma_{33}^b, \quad \sigma_{33}^b = \sigma_{23}^b = 0. \tag{3}$$

By modifying Eq. (2) and incorporating the boundary conditions (Eq. (3)), a relationship in the following form can be obtained [14].

$$B^I = MA, \tag{4}$$

where

$$B^I = \begin{bmatrix} 0 & 0 & 0 & 0 & u_1^I & \sigma_{33}^I \end{bmatrix}^{\mathrm{T}},$$

$$M = \begin{bmatrix} 1 & 0 & t_{11} & t_{12} & 0 & s_1 \\ 0 & 1 & t_{21} & t_{22} & 0 & s_2 \\ 0 & 0 & t_{51} & t_{52} & 0 & s_5 \\ 0 & 0 & t_{61} & t_{62} & 0 & s_6 \\ 0 & 0 & t_{31} & t_{32} & a_1 & s_3 \\ 0 & 0 & t_{41} & t_{42} & a_2 & s_4 \end{bmatrix} \quad \text{and} \quad A = \begin{bmatrix} u_1^t & u_2^t & u_1^b & u_2^b & A_1^r & A_1^t \end{bmatrix}^{\mathrm{T}},$$

where superscript t and b stand for top and bottom, respectively, t_{1j} are the corresponding element of transfer-matrix T, u_i^t and u_i^b are the displacements of the multi-layered laminate at the upper interface and the lower interface, respectively, A_1^r and A_1^t are the reflected and transmitted coefficient, s_i are product terms, and U_i^t and U_i^b are the unit displacement vectors of the reflected wave in the upper substrate and the transmitted wave in the lower substrate, respectively. More details on the formulation are available elsewhere [8].

The determinant of M must be zero for a non-zero solution of A.

$$\det(M) = 0. \tag{5}$$

In general for a given frequency and plate thickness, the roots (k_1) of the above equation are complex. The inverse of the real part of the root $\mathrm{Re}(k_1)$ represents the phase velocity of the leaky guided plate wave while the imaginary part of the root $\mathrm{Im}(k_1)$ is the attenuation of the plate wave. It should be noted that the attenuation of leaky plate waves consists of two parts: one is due to the visco-elastic property of the material, which absorbs the energy of the plate wave, and the other represents the energy leaked to the surrounding fluid.

3. The guided wave power flow vector

The power flow (energy reflection and energy transmission vector obtained from the Poynting vector) can be defined as [17]

$$p_i^{\alpha} = \frac{1}{2}\,\sigma_{ij}^{\alpha} v_j^{\alpha *}, \tag{6}$$

where v_i^{α} is the ith component of the velocity for the wave mode α obtained by taking the derivative of particle displacements with respect to time t as $v_i^{\alpha} = -\mathrm{j}\omega u_i^{\alpha}$ and $\sigma_{ij}{}^{\alpha}$ is the associated stress component obtained through the generalized Hooke's law as $\sigma_{ij}^{\alpha} = C_{ijkl}\varepsilon_{kl}^{\alpha}$. Summation over repeated index is implicit in the above expression for the power flow. For each lay-up, the power flow magnitude and direction of each partial wave mode is determined in each layer. It is known that guided waves in a plate are made up of partial bulk waves. It follows that the energy of the guided wave in a plate can be expressed as a superposition of bulk wave energies. For a multi-layer plate, it is anticipated that the guided plate waves are generated on the basis of superposition of the power/energy distribution (magnitude and direction), of the partial bulk wave modes, in each super-layer group [29].

4. Beam model simulation

It is assumed in this model that each partial wave mode is provided an equal opportunity to generate a guided wave mode in the direction of the power flow vector. The energy value calculated from the plane wave mode is considered to have a Gaussian distribution centered about the power flow direction. Thus, the energy value at each grid point, in a plate (see Fig. 2) was computed using:

$$E_g(x,y) = \sum_{\alpha=1}^{m}\sum_{i=1}^{n} \frac{p_i^{\alpha}}{r\sqrt{2\pi\beta}}\,\mathrm{e}^{-d^2/2\beta}. \tag{7}$$

In this equation, $p_i{}^{\alpha}$ is the energy value of a partial wave mode at each layer and is obtained from the magnitude of the power flow vector using Eq. (6); n is the number of the layers; m is the number indicating the partial wave mode; r is the distance between the grid point and the source; d is the distance of the grid point from the beam center; ψ is the angle of divergence, and β is the variance considered as a function of r and Ψ and given by

$$\beta = \beta_{\mathrm{init}} + r^2\cos^2(\Psi). \tag{8}$$

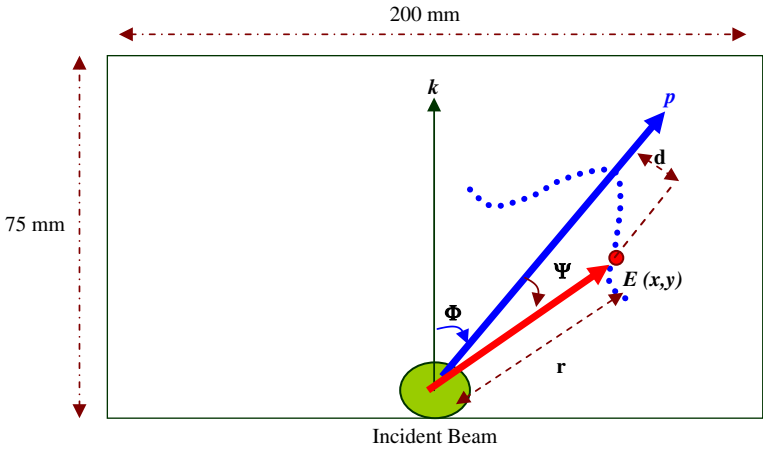

Fig. 2. The description of the Gaussian beam model for simulating the PWFP images showing the wave vector (**n**) and the pointing vector (**p**) directions.

Here, β_{init} is an initial variance value empirically determined. The theoretical PWFP image is obtained by plotting the $E_g(x, y)$ function using a gray scale to represent the magnitude.

5. Simulation results and discussion

The experimental studies of plate wave propagation in composite laminates have been reported earlier [5–7] and hence will be only briefly described here. The experimental setup used, is shown in Fig. 3. Here, two piezoelectric immersion transducers (manufactured by Panametric Inc., USA), with narrow frequency bandwidth, were used in an immersion-scanning tank. The transmitting probe was fixed while the receiving probe was moved in a raster pattern across the laminate. The incidence angles for both the probes were fixed, and in the case studies discussed and an incidence angle (θ) of 10° from the normal to the plate was selected and the results have been earlier reported [7]. The azimuthal angles (φ) of the two probes were fixed at 0°. Graphite epoxy composite laminates, manufactured using an autoclave based ply lay-up procedure, were examined. The specimens were of the same thickness of 2.72 mm each and were made up of 20 unidirectional graphite-epoxy laminae. The lay-up patterns of the specimens were: $A = (45_5/-45_5)_s$, $B = (90_2/+45_4/-45_4)_s$, and $C = (60_5/-30_5)_s$ where the 0° angle is along the direction of wave vector of the transmitter (i.e. perpendicular to the face of the transmitter). The elastic constants for the layers, used in the theoretical analysis, were obtained from experiments using ultrasonic velocity measurements conducted at 1 MHz [6,7], and is provided in Table 1.

The multi-layered model was used to obtain the energy distribution plots for the individual partial wave modes in each layer. There are six partial wave modes in each layer. Only the three partial wave modes with energy vector having components in the $+z$ direction were considered, since in the experimental setup, the receiving probe was on the same side of the specimen as the transmitter. The quasi-longitudinal partial wave mode is indicated by the L_1 and the two quasi-transverse partial wave modes are indicated by T_s and T_f.

Fig. 4 shows the computed plate wave flow patterns in unidirectional composite plates with fiber orientation at 0° and 60° angles with respect to the axis of incidence (excitation) represented by the wave vector **k**. It is observed that the model predicts that the maximum energy of the guided plate wave beam traveling in the plate tends to follow the direction of the fibers in the unidirectional fiber reinforced composite and skews away from the incident direction. The model also illustrates that the relative energy density for the case in Fig. 4a where the fiber is along the same direction as the incident beam, is higher relative to the case in Fig. 4b where

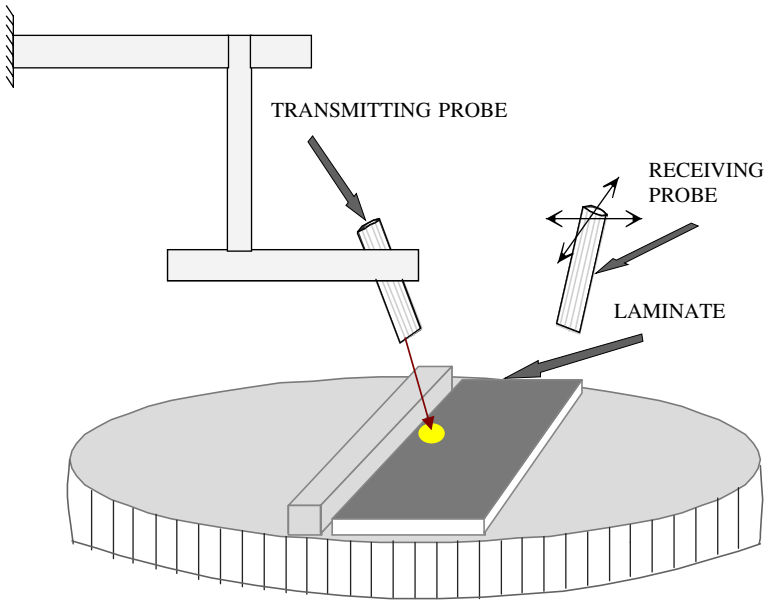

Fig. 3. The experimental setup used for obtaining the PWFP images from graphite-epoxy plates.

Table 1
Material property of the graphite epoxy fiber composite layer

ρ (10^3 kg/m^3)	1.55
C_{11}(GPa)	110.7
C_{12}(GPa)	7.5
C_{22}(GPa)	14.1
C_{13}(GPa)	7.5
C_{33}(GPa)	14.1
C_{23}(GPa)	7.3
C_{44}(GPa)	3.37
C_{55}(GPa)	6.1
C_{66}(GPa)	6.1

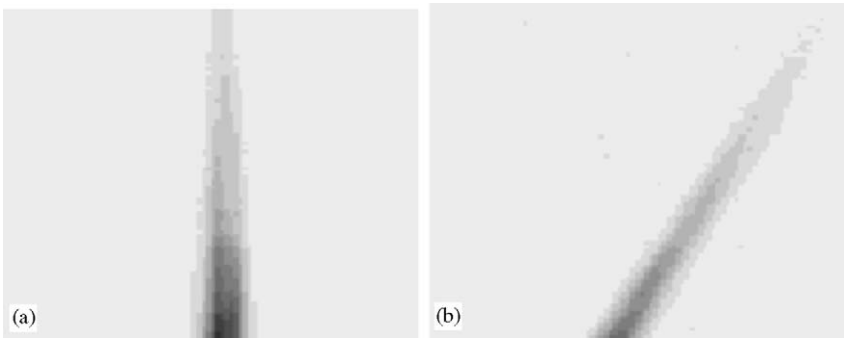

Fig. 4. The simulated power flow pattern for unidirectional graphite epoxy plate with the wave vector, (a) along the fiber direction and (b) at 60° to the fiber direction. Here, the wave vector points along the vertical axis and the dark color indicates high pointing energy.

the fibers are at an angle. The model predictions compare well with the experimental results that have been reported elsewhere by the authors [6,7] and by others [30] for the unidirectional fiber reinforced composites. It must be noted here that the beam skewing is due to the anisotropy of the plate that is caused by the fibers that have a high stiffness along the length.

The beam skewing phenomena can be explained using the slowness curves as illustrated by the schematic representation in Fig. 5. Here, a typical slowness curve for a highly anisotropic media such as the unidirectional fiber reinforced composite plate is shown at a fiber orientation of 60° to the incidence plane indicated by the wave vector **k**. The direction of the energy flow is obtained from the normal to the slowness surface as indicated by the vector **p** which tends to follow an angle that is different from the vector **k** for this case. The angle between **k** and **p** is often called as the beam skew angle.

Four cases for the wave propagation in multi-directional ply composites were studied for the comparison between theoretical results and experimental results of the PWFP images. Figs. 6(a) and (b) show both theoretical and experimental results of guided wave propagation in Laminate *A* using a frequency of 1 MHz that are comparable except that the beams are sharp in the model predictions when compared to the experiments. It should be noted that besides the two strong power flow propagation patterns along approximate the 42° orientation; there are also weaker beam propagation along smaller angles. The analysis of the Poynting vector magnitudes and orientation (discussed in more detail later) indicate that the stronger beams are combined by quasi-longitudinal partial waves (40°) and fast quasi-shear partial waves (32°), while the weaker beams are slow quasi-shear partial waves. Fig. 6d shows the theoretical result of the guided waves propagation in Laminate *A* using a frequency of 0.5 MHz. From the image one can see that most of the energy propagates along the 45° layers. This agrees with the experimental results shown in Fig. 6c.

For a frequency of 1 MHz, the results in Figs. 6(e) and (f) show the guided wave propagation in Laminate *B*, and Figs. 6(g) and (h) represent guided waves energy patterns in Laminate *C*. As before, in both cases the theoretical results are similar to the experimental results. For specimen *C* $\{60_5/150_5\}_s$ the T_f partial mode at

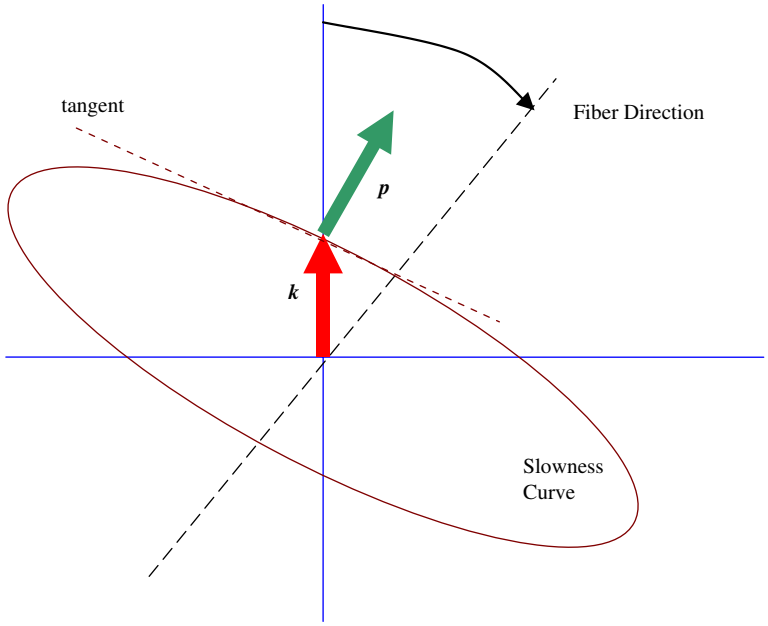

Fig. 5. Schematic illustrating the orientation of the energy vector with respect to the wave propagation on a slowness curve for the case where the fiber is oriented at an angle θ to the axis of symmetry. Here, the slowness curve is for an arbitrary material.

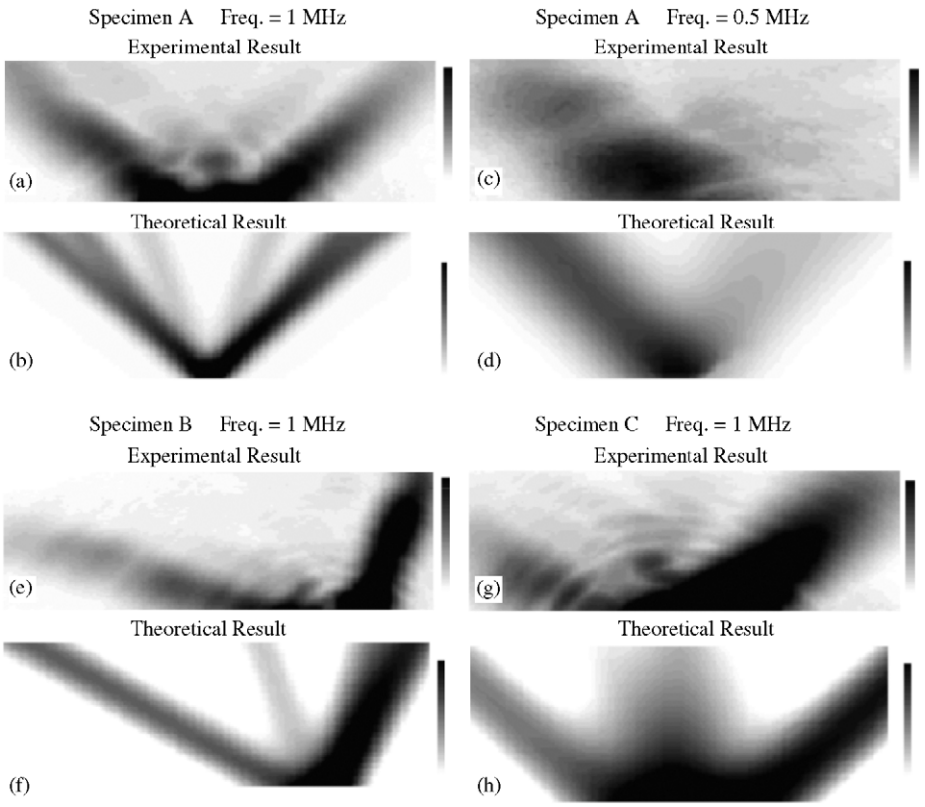

Fig. 6. The comparison of the model-based Plate Wave Flow Patterns (PWFP) with experimental results for different ply orientations with respect to the axis of guided wave generation (which is along the vertical). Here, dark regions represent regions of high energy flow.

around -25° azimuthal angle is the dominating partial mode in the middle ply group. Also, L_1 partial mode is the predominant partial mode in the outer layers and propagates along $+53^\circ$ and has less energy when compared with the T_f partial mode in the middle layer. This is clearly manifested in the PWFP experiments and even the weak T_s partial mode along the -12° is visible.

The beam behavior in the multi-layered anisotropic media could be explained using the magnitude and the orientation of the Poyntng vector in the individual plies that is obtained from the model. In Fig. 7a, the magnitude of the average power flow vector (energy) for individual plies in specimen A with $\{45_5/-45_5\}_s$ ply lay-up is presented as a function of distance into the specimen (x_3). The three-ply groups (upper—$\{+45^\circ\}$, lower—$\{-45^\circ\}$, and the bottom—$\{+45^\circ\}$) are clearly distinguishable. It must be noted here that these plots is a graphical representation of the average per ply energy magnitude and direction as represented in Table 2 and not the exact distribution of the energy as a function of depth. Here, L_1 represents the two partial modes of quasi-longitudinal bulk wave modes. Similarly, T_f is the fast quasi-transverse partial wave modes while T_s is the slow quasi-transverse partial wave modes. It is observed that the magnitude of energy is maximum for the T_f mode in the middle layer while the other two modes are relatively weak. Also in the outer layer, there is an even energy distribution of the three mode types with T_f and L_1 higher than the T_s partial mode. Using Fig. 7b, the orientation of these partial modes in the azimuthal (1–2 or x–y) plane is predicted. From this graph, the T_f in the middle layer is predicted to be at an angle of approximately 132° (or -42°) which incidentally is along the fiber direction in the middle ply group and is also observed in the experimentally obtained plate wave flow

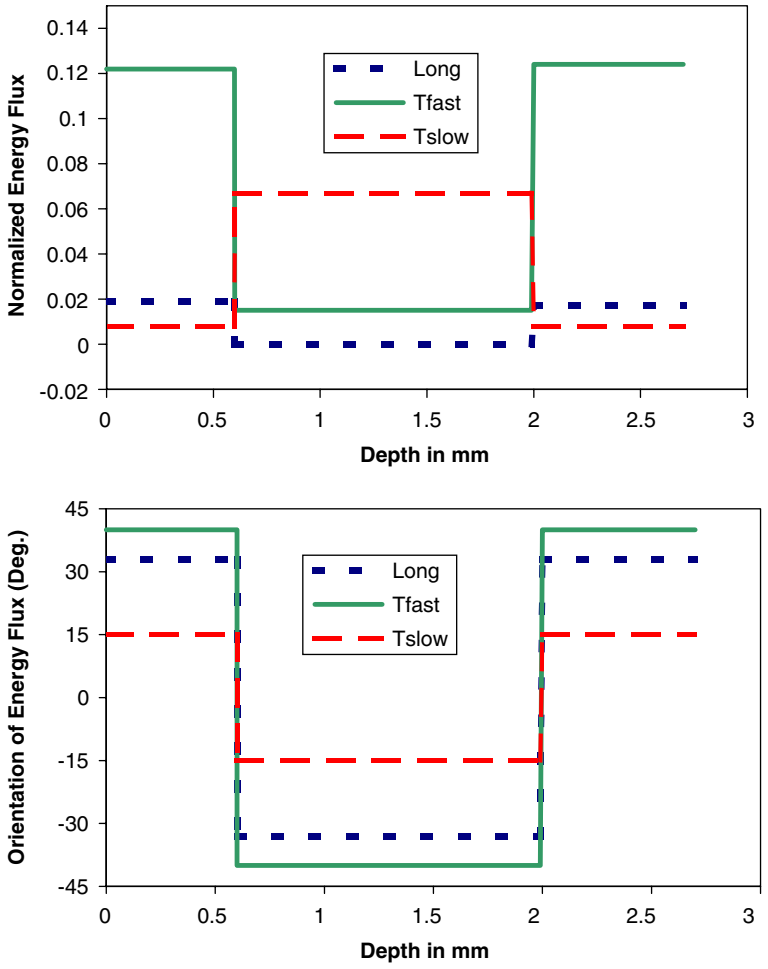

Fig. 7. The power flow vector magnitude and direction in a three "super-layer" graphite-epoxy plate specimen A $(+45_5, -45_5)_s$ for the three partial wave.

Table 2
Numerical results of guided waves propagation in $A(+45_5/-45_5)_s$ laminate at 1 MHz frequency

Partial wave mode type	Average propagation angle (Φ) degree			Power flow magnitude (p_j^j) GW/m^2		
	+45 Layer	−45 Layer	+45 Layer	+45 Layer	−45 Layer	+45 Layer
Longitudinal (L)	40	−40	40	0.07	0.06	0.02
Transverse fast (T_f)	32	−32	32	0.06	0.05	0.02
Transverse slow (T_s)	17	−17	17	0.09	0.04	0.02

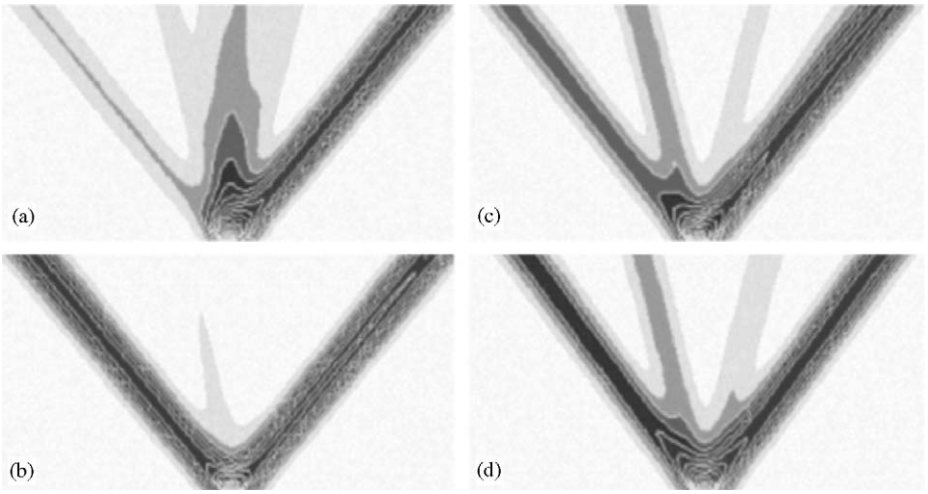

Fig. 8. Power flow distribution prediction using the model for different wave modes as a function of frequency × thickness product in specimen A: (a) A0 mode at $f \times d = 0.785$ MHz mm, (b) A0 mode at $f \times d = 0.950$ MHz mm (c) S0 mode at $f \times d = 1.05$ MHz mm and $Vp = 4578$ m/s and (d) S0 mode at $f \times d = 1.20$ MHz mm.

pattern results (Fig. 6c). In the outer layers, the direction of T_f and L_1 are both approximately equal to 40° which again is almost along the fiber direction. This is again visible in the PWFP shown in Fig 6. The weak T_s is also visible, although not as clearly (due to low amplitude) along the 17° in the outer layers and −18° in the middle ply group as predicted by theory in Fig. 6b.

In Fig. 8, additional results have been included based on models. Here, since the intent was not to compare experimental results, the individual guided wave modes were studied using the models. Both S0 and A0 modes were observed at two different frequencies. It can be observed that while there features of the preferred orientation of energies along the four angles are similar, there are significant differences in the relative energy partitioning for each case. For instance, in Fig. 8a the primary angles of energy propagation are 0° and +45°, while for all other three cases the primary angles are +45° and −45°. For the case in Fig. 8b there is significantly less energy along the 0° when compared to Fig. 8a showing that small changes in the frequency for the same mode will lead to relatively large effects on the energy partitioning in these strongly anisotropic plates.

6. Conclusions

A model using a Gaussian beam approximation to a plane wave transfer-matrix model for a multilayered composite plate was used to generate predictions of guided wave behavior in anisotropic material systems such as the reinforced composites. It is clear from the above analysis that ultrasonic guided wave generation and propagation are strongly influenced by the anisotropy of the propagating media (that is caused by the fiber-reinforced composites here). The proposed model predicts that guided wave beam skewing and beam splitting

phenomena are quite complex in multi-layered fiber-reinforced anisotropic plates as has been observed and reported [5–8]. While it can be anticipated that in a unidirectional fiber reinforced composite material, the guided-wave energy flow would be governed by the corresponding slowness curves, as has been demonstrated in Ref. [30], it is significant to note that the model proposed here, that is based on Poynting vector approach based on transfer-matrix approach, predicts that in a fiber-reinforced laminate energy flow patterns are strongly influenced by the anisotropy in each individual layer of the laminate. The correlation between the experimental results and the model prediction shows that the energy propagation of guided wave modes in structurally anisotropic media could indeed be considered as governed by the power flow distribution (Poynting vector) of individual partial wave modes. The description of plate flow patterns by a model based on individual partial waves is considered fundamental, albeit phenomenological, since these individual partial waves constitute the guided waves in plates and since use of the transfer-matrix method ensures correct coupling of these individual waves across the distinct layers. The model assumes a lossless media. While attenuation is expected to be directional in such materials, the visco-elastic component, not modeled due to the non-availability of the appropriate visco-elastic constants, may explain the ''diffusion'' of energy (lack of sharpness) in the neighborhood of preferred flow directions in the experimental results that is not found in the theoretical predictions.

References

[1] M.J.P. Musgrave, The propagation of elastic waves in crystals and anisotropic media, *Reports on Progress in Physics* 22 (1959) 74–96.
[2] J.L. Rose, K. Balasubramaniam, A. Tverdokhlebov, A numerical integration Green's function model for ultrasonic field profiles in anisotropic media, *Journal of NDE* 8 (3) (1989) 165–179.
[3] P. Jeong, Ultrasonic Characterization of Centrifugally Cast Stainless Steel, EPRI Report, NP-5246, 1987.
[4] D.S. Kupperman, K.J. Reimann, J. Abrego-Lopez, Ultrasonic NDE of cast stainless steel, *NDT International* 20 (3) (1987).
[5] R. Sullivan, K. Balasubramaniam, A.G. Bennett, Experimental imaging of fiber orientation in multi-layered graphite epoxy composite structures, in: D.O. Thompson, D.E. Chimenti (Eds.), *Review of Progress in Quantitative Nondestructive Evaluation*, Vol. 13, Plenum Press, NY, 1994, pp. 1313–1320.
[6] R. Sullivan, Ultrasonic Imaging of Ply Orientation in Graphite Epoxy Laminates using Oblique Incidence Techniques, MS Thesis, Mississippi State University, MS 39762, 1993.
[7] R. Sullivan, K. Balasubramaniam, A.G. Bennett, Plate wave flow patterns for ply orientation imaging in fiber reinforced composites, *Materials Evaluation* 54 (4) (1996) 518–523.
[8] Y. Ji, Theoretical modeling of ultrasonic wave propagation in generally anisotropic viscoelastic multi-layered composite laminates, PhD Dissertation, Mississippi State University, MS 39762, 1996.
[9] K. Balasubramaniam, Y. Ji, Guided wave analysis in inhomogeneous plates, in: D.O. Thompson, D.E. Chimenti (Eds.), *Review of Progress in QNDE*, Vol. 14, Plenum Press, NY, 1995, pp. 227–234.
[10] K. Balasubramaniam, Y. Ji, Analysis of acoustic energy transmission through anisotropic wave guides using a plane wave multi-layer model, in: P.K. Raju, R. Gibson (Eds.), *Materials For Noise and Vibration Control*, NCA-Vol-18, DE-Vol-80, ASME Publisher, New York, 1994, pp. 157–163, ISBN#0-7918-1459-8.
[11] Y. Ji, R. Sullivan, K. Balasubramaniam, Review of progress in QNDE, in: D.O. Thompson, D.E. Chimenti (Eds.), *Guided Wave Behavior Analysis in Multi-layered Inhomogeneous Anisotropic Plates*, Vol. 15, Plenum Press, NY, 1996.
[12] K. Balasubramaniam, Y. Ji, Analysis of ultrasonic plate wave interaction with multi-layered inhomogenous anisotropic plates, *Proceedings of the First US-Japan Symposium on Advances in NDT*, June 24–28, 1996, Kahuku, Oahu, HA, pp. 216–217.
[13] M. Lowe, Matrix techniques for modeling ultrasonic waves in multilayered media, *IEEE Transactions on Ultrasonics Ferroelectrics and Frequency Control* 42 (1995) 525–542.
[14] W.T. Thomson, Transmission of elastic waves through a stratified solid medium, *Journal of Applied Physics* 21 (1950) 89.
[15] N.A. Haskell, The dispersion of surface waves in multi-layered media, *Bulletin of the Seismological Society of America* 43 (1953) 17–34.
[16] L.M. Brekhovskikh, *Waves in Layered Media*, Academic Press, New York, 1960.
[17] B.A. Auld, *Acoustic Fields and Waves in Solids*, second ed., Vols. 1 and 2, Robert E. Krieger Publishing Company, Malabar, Florida, York, NY, 1990, pp. 39–52.
[18] S.I. Rokhlin, T.K. Bolland, L. Adler, Reflection and refraction of elastic waves on a plane interface between two generally anisotropic media, *Journal of the Acoustic Society of America* 79 (4) (1986) 906–918.
[19] A.H. Nayfeh, *Wave Propagation in Layered Anisotropic Media*, Amsterdam, North-Holland, 1995.
[20] T.C.T. Ting, *Anisotropic Elasticity*, Oxford University Press, Oxford, 1996.
[21] A.K. Mal, Y. Bar-Cohen, Ultrasonic characterisation of composite laminates, in: A.K. Mal, T.C.T. Ting (Eds.), *Wave Propagation in Structural Composites*, *AMD-90*, American Society of Mechanical Engineers Press, New York, 1988.
[22] B. Hosten, Reflection and transmission of acoustic plane waves on an immersed orthotropic and viscoelastic solid layer, *Journal of the Acoustic Society of America* 89 (6) (1991) 2745.

[23] S.K. Datta, A.H. Shah, T. Chakraborty, R.L. Bratton, Wave propagation in laminated composite plates: anisotropy and interface effects, in: A.K. Mal, T.C.T. Ting (Eds.), *Wave Propagation in Structural Composites, AMD-90*, American Society of Mechanical Engineers Press, New York, NY, 1988, pp. 17–29.

[24] M. Castaings, B. Hosten, Delta operator technique to improve the Thomson–Haskell-method stability for propagation in multilayered anisotropic absorbing plates, *Journal of the Acoustic Society of America* 95 (1994) 1931.

[25] L. Wang, S.I. Rokhlin, Stable reformulation of transfer-matrix method for wave propagation in layered anisotropic media, *Ultrasonics* 39 (6) (2001) 413–424.

[26] K. Balasubramaniam, Wave reflection/transmission analysis of thick multi-layered structures using the numerical truncation approximation for the transfer-matrix technique, *Proceedings of the ASME Noise Control and Acoustics Division*, NCA-Vol. 26, 1999, pp. 279–285.

[27] K. Balasubramaniam, On a numerical truncation algorithm for transfer-matrix method, *Journal of the Acoustic Society of America* 107 (2) (2000) 1053–1056.

[28] K. Balasubramaniam, M.M. Vikram, V. Reddy, A comparison of ultrasonic wave reflection/transmission models from isotropic multi-layered structures by transfer-matrix and stiffness matrix recursive algorithms, in: D.O. Thompson, D.E. Chimenti (Eds.), *Review of Progress in Quantitative Nondestructive Evaluation*, Vol. 22, AIP Conference Proceedings, Vol. 657, 2003, p. 1095.

[29] K. Balasubramaniam, Y. Ji, Influence of skewing on the acoustic wave energy vector behavior in anisotropic material systems, *Journal of Sound and Vibration* 236 (1) (2000) 166–175.

[30] S. Baly, C. Potel, J.-P. de Belleval, M. Lowe, Numerical and experimental deviation of monochromatic lamb wave beam for anisotropic multi-layered media, in: D.O. Thompson, D.E. Chimenti (Eds.), *Review of Progress in Quantitative Nondestructive Evaluation*, AIP Proceedings, CP615, Vol. 21, 2002, pp. 270–278.